Neural Comput & Applic (2017) 28:4123–4137
DOI 10.1007/s00521-016-2316-6

ORIGINAL ARTICLE

Dynamical balance optimization and control of biped robots in double-support phase under perturbing external forces

Liyang Wang[1] · Yongyong Ge[2] · Ming Chen[1] · Yongqing Fan[3]

Received: 25 November 2014 / Accepted: 4 April 2016 / Published online: 18 April 2016

Abstract To realize the dynamic balance optimization and control of biped robots under the perturbing external forces in the double-support phase, a systematic scheme is proposed in this paper. First, a constrained dynamic model of biped robots and a reduced order dynamical model for the double-support phase are formulated. Considering the dynamic external wrench applied on biped robots, we present a dynamic force distribution approach based on quadratic objective function for computing the optimal contact forces to equilibrate the dynamic external wrench. As a result, the sum of the normal force components is minimized for enhancing safety and energy saving. Then, one primary recurrent neural network (RNN) is adopted to solve the optimization problem subject to both equality and inequality constraints. For the derived optimized contact force and motion, hybrid motion/force control is proposed based on another RNN to approximate unknown dynamic functions. Adaptive learning algorithms for learning the parameters of the RNN are provided as well. The proposed control can deal with the uncertainties including approximation errors and external disturbances. Extensive simulations are presented to demonstrate the effectiveness of the proposed optimization and control approach.

Keywords Biped robots · Dynamic force distribution · Balance optimization · Motion/force control

✉ Liyang Wang
ddd0wwl@sohu.com

[1] Department of Electronic Engineering, Shunde Polytechnic, Foshan Guangdong, China

[2] College of Engineering, Peking University, Beijing, China

[3] School of Automation, Xi'an University of Posts and Telecommunications, Xi'an 710121, China

1 Introduction

The biped robot locomotion attracts much attention from the research community [1–8]. A biped robot is not fixed to the floor, while it must be able to interact with the environment through multiple contacts to maintain dynamic balance and enhance its flexibility, dexterity, and functionality so as to follow and work with human autonomously. Therefore, the dynamic balance control for biped robots is particularly important. Ground reaction force for the biped legs must be regulated to maintain dynamic balance that is robust to unknown disturbances. In this respect, several research results have been reported. In [9], a kind of dynamically stable and collision-free trajectories are planned for full-body posture goals of biped robots. In [10], control design was constructed for stabilization of non-periodic trajectories of underactuated robots traversing rough or uneven terrain. In [11], a simple balance control algorithm compatible with a typical walking control system in the 2D plane was proposed. In [12], the authors constructed an efficient control using implicit function with support vector regression-based data-driven model for holonomic constrained under-actuated biped robots.

Different from performance indicators of manipulators and vehicles, good performance for a walking robot can be simply defined as maintaining the dynamic balance during its locomotion [13–19]. In this respect, the main control objective of a walking robot is to guarantee a suitable ground reaction force to maintain the dynamic balance, and it is also desirable to have a controller that allows the robot to adapt (compliantly) to unknown external forces. Traditionally, a general strategy is to use the dynamics based walking pattern generation which provides the desired trajectories for underlying position controllers [20–23]. In [24], a locomotion control system using nonlinear

oscillators for a biped robot was proposed to achieve robust walking. In [25], an approach was proposed to find stable as well as unstable hybrid limit cycles for a planar compass-like biped on a shallow slope without integrating the full set of differential equations and approximating the dynamics. In [2], an approach for the closed-loop control of a fully actuated walking biped that leverages on its natural dynamics was presented, and the input state-dependent torques were built using a combination of low-gain spring-damper couples. Researches were also made to construct complete models to represent the whole periodic walking motion and three phases of the walking cycle (single-support, double-support, and transition phase). The performance and stability analysis of the whole closed-loop motion system are improved because that the integrated biped model is studied carefully [26, 27]. On the other hand, to maintain dynamic balance in various situations, learning algorithms for biped walking were presented in [28–32].

For biped robots, appropriate ground reaction forces are necessary to guarantee the dynamic balance especially when there are disturbances of external wrenches (forces and moments) including the gravity force and the inertia wrench exist. Since each toe and heel are independently characterized by non-penetration and no-slip constraint with the ground, and the external wrench is usually time-varying, the contact forces must satisfy certain constraints and be solved in real time to balance the change of the external wrench, typically the friction cone constraint such that it can be feasible. Therefore, how to determine the existence of feasible contact forces to resist an external wrench and maintain the system's equilibrium need to be considered. On the other hand, for a resistable external wrench, there will be infinite solutions to counterbalance it, since there are many configurations. Then some optimization criterion should be adopted in computing the contact forces, usually to minimize their overall magnitude.

To perform dynamic balance control for the biped, the result of contact-force optimization must be used in the control law, and thus, the optimal force-distribution problem can be solved in real time. Parallel and distributed approaches to contact-force optimization for the biped are deemed necessary and desirable. In recent years, neural network-based approaches have demonstrated their great promise for optimization. Neural networks for constrained optimization problems have been widely explored for real-time applications [33]. Reported results of numerous investigations have shown many advantages over the traditional optimization algorithms, especially in real-time applications [34].

In this paper, we consider dynamical balance optimization and biped locomotion in double-support phase. The biped robot usually starts and stops motion at the double-support configuration. The analysis of biped locomotion in the double-support phase is very important for improving the smoothness of the biped locomotion system and dynamic balance [35]. This paper investigates the dynamic balance optimization and control of biped robots with the perturbing external forces in the double-support phase. First, we formulate a constrained dynamic model of the biped robot and a reduced order model for the double-support phase. Considering the dynamic external wrench on the biped, a dynamic force distribution approach based on quadratic objective function [36] is proposed for computing the optimal contact forces to equilibrate a dynamic external wrench, such that the sum of the normal force components is minimized for enhancing safety and energy saving. Then, a primary recurrent neural network (RNN) with self-stabilizing ability is adopted to deal with the complicated optimization problem subject to both equality and inequality constraints. For the obtained contact forces and desired trajectories, we propose the hybrid motion/-force control based on the second RNN to approximate unknown dynamic functions with the adaptive weight parameters updating, and the adaptive learning algorithms that can learn the parameters of the RNN are derived using Lyapunov stability theorem. The proposed control can confront the uncertainties including approximation error, optimal parameter vectors, higher-order terms in Taylor series, and external disturbances. The verification of the proposed control is conducted using extensive simulations.

2 Dynamics of biped robots

The constraints for the biped robot in the double-support phase are assumed to be holonomic, arising from geometrical constraints on the joint coordinates. For a biped robot with n joint coordinates q and n input torques τ, these constraints can be represented by

$$\Phi(q) = 0 \tag{1}$$

where $\Phi \in R^m$, and m is the dimension of the constraints, for example, $m = 3$ for a two-dimensional (2-D) biped model and $m = 6$ for a three-dimensional (3-D) model. Define the augmented Lagrangian

$$L = K - P + f^T \Phi \tag{2}$$

where K is the total kinematic energy, P is the potential energy, and f is an m-vector of constraint force. The equations of motion can be written as

$$\frac{\mathrm{d}}{\mathrm{d}t}\frac{\partial L}{\partial q} - \frac{\partial L}{\partial q} = \tau \tag{3}$$

Thus, the dynamic equations of the biped robot in the double-support phase can be represented by

$$M(q) + C(q,\dot{q})\dot{q} + G(q) = \tau + J^T f \tag{4}$$

$$M = [m_{kj}]_{k=1,\ldots,n;j=1,\ldots,n} \tag{5}$$

$$C(q,\dot{q}) = \left[\sum_{i=1}^{n} \frac{\partial m_{kj}}{\partial q_i} + \frac{\partial m_{kj}}{\partial q_j} - \frac{\partial m_{kj}}{\partial q_k}\right]_{k=1,\ldots,n;j=1,\ldots,n} \tag{6}$$

$$G(q) = \frac{\partial P}{\partial q} \tag{7}$$

$$J = \frac{\partial \Phi}{\partial q} \tag{8}$$

where $M(q) \in R^{n\times n}$ is a symmetric positive definite inertia matrix, $C(q,\dot{q}) \in R^{n\times n}$, $G(q) \in R^n$, and $J \in R^{m\times n}$.

When the biped is in the double-support phase, the number of DOF becomes $(n - m)$ and the left m DOF contribute to the contact forces. We assume that the constraints can be written as

$$\Phi(q) = \Phi_1(q_1) - \Phi_2(q_2) = 0 \tag{9}$$

where q_1 are $(n - m)$ independent coordinates and q_2 are m constraint coordinates. The physical interpretation of this assumption is that the position and orientation of the biped body can be calculated either starting from the left foot or the right foot, and each involves either of the joint coordinates q_1 or q_2. By differentiating (9), we obtain

$$J(q)\dot{q} = J_1(q_1)\dot{q}_1 + J_2(q_2)\dot{q}_2 = 0 \tag{10}$$

where

$$J = \left[\frac{\partial \Phi}{\partial q_1}, \frac{\partial \Phi}{\partial q_2}\right] = [J_1, J_2] \tag{11}$$

and $J_1(q_1) = \partial\, \Phi / \partial\, q_1$, and $J_2(q_2) = -\partial\, \Phi / \partial\, q_2$, with $J_1 \in R^{m\times(n-m)}$ and $J_2 \in R^{m\times m}$, implying that

$$\dot{q}_2 = \frac{\partial q_2}{\partial q_1}\dot{q}_1 = -J_2^{-1}J_1\dot{q}_1 \tag{12}$$

The generalized displacement and velocity can be expressed in terms of the independent coordinates q_1 and $\dot{q}_1$, as

$$q = [q_1^T, q_2^T]^T \tag{13}$$

$$\dot{q} = \begin{bmatrix} I_{n-m} \\ -J_2^{-1}J_1 \end{bmatrix}\dot{q}_1 = H(q)\dot{q}_1 \tag{14}$$

Due to the velocity transformation (14), the generalized acceleration satisfies $q = H(q)q_1 + \dot{H}(q)\dot{q}_1$. The motion (4) is further represented by the independent coordinates q_1, $\dot{q}_1$, and q_1 as

$$M(q)H(q)q_1 + \big(M(q)\dot{H}(q) + C(q,\dot{q})H(q)\big)\dot{q}_1 + G(q) = \tau + J^T f \tag{15}$$

Remark 2.1 By (15), there is an actuator redundancy because the dimension of the control input is larger than that of the controlled output. The extra dimension of actuators should be used to produce the ground reaction force, which can balance the external dynamic wrench.

Lemma 2.1 [37] *Let* e = H(s)r *with* H(s) *representing an* $(n \times m)$*-dimensional strictly proper exponentially stable transfer function, and r and e denoting its input and output, respectively. Then* $r \in L_2^m \cap L_\infty^m$ *implies that* $\dot{e} \in L_2^m \cap L_\infty^m$, *e is continuous, and* $e \to 0$ *as* $t \to \infty$. *If, in addition,* $r \to 0$ *as* $t \to \infty$, *then* $\dot{e} \to 0$.

Lemma 2.2 *Given a differentiable function* $\phi(t) : \mathbb{R}^+ \to \mathbb{R}$, *if* $\phi(t) \in L_2$ *and* $\dot{\phi}(t) \in L_\infty$, *then* $\phi(t) \to 0$ *as* $t \to \infty$, *where* L_∞ *and* L_2 *denote bounded and square integrable function sets, respectively.*

The dynamic system (4) has the following properties [37].

Property 2.1 Matrices $M(q)$, $G(q)$ are uniformly bounded and uniformly continuous if q is uniformly bounded and continuous. Matrix $C(q,\dot{q})$ is uniformly bounded and uniformly continuous if $\dot{q}$ is uniformly bounded and continuous.

Property 2.2 Matrix $\dot{M} - 2C$ is skew-symmetric. i.e., $x^T(\dot{M} - 2C)x = 0$, $\forall x \neq 0$

3 Dynamical balance optimization

Consider double-support phase shown in Fig. 1, of the biped in a 3-D workspace with i point contacts between the ground and the feet, fixed with a right-handed coordinate frame. Assume that each foot contacts the ground with Coulomb friction. Let n_i, o_i, and t_i be the unit inward

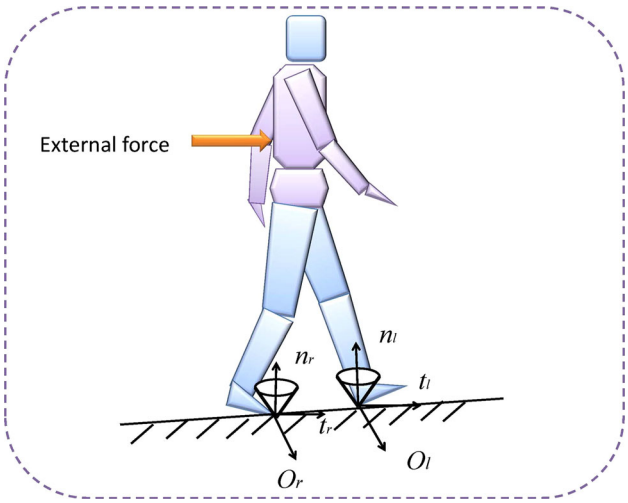

Fig. 1 Double-support phase

normal and two unit tangent vectors at contact $i(i = l, r)$, where l denotes the left leg, and r denotes the right leg, in the COM coordinate frame such that $n_i = o_i \times t_i$. The contact force f_i can be expressed in the local coordinate frame $\{n_i, o_i, t_i\}$ by

$$f_i = [f_{in}, f_{io}, f_{it}]^{\mathrm{T}} \tag{16}$$

where f_{in}, f_{io}, and f_{it} are the components of f_i along n_i, o_i, and t_i, respectively.

A contact force $f_i \in R^{\kappa}$ is applied by each foot to the ground to hold the biped without slippage and tip-over, and balance with any external forces. To ensure nonslipping at a contact point, with the contact normal along z direction and directed outward and a Coulomb friction coefficient μ_i at contact i, the contact force f_{in} must satisfy the contact constraint

$$\sqrt{f_{io}^2 + f_{it}^2} \le \mu f_{in} \tag{17}$$

where μ is the static friction coefficient of the substrate. The friction constraint can be geometrically represented as a cone with its axis orthogonal with respect to the support surface and with an "opening angle" equal to $\alpha = \arctan(\mu)$.

In order to overcome the nonlinearities induced by the friction cone equations, it is possible to substitute the friction cone with an inscribed pyramid (see Fig. 1). Hence, we have a more restrictive constraint, expressed by

$$\|f_{io}\| \le \mu_p f_{in}, \|f_{it}\| \le \mu_p f_{in} \tag{18}$$

where $\mu_p = \mu/\sqrt{2}$.

A definite foot contacts with the ground, only if there is an f_{in} such that

$$f_{in} \ge 0 \tag{19}$$

Concerning the adhesion constraint, it can be satisfied if the absolute value of the sum of the distributed forces is less than the maximum allowable friction force. The friction force constraints may be rewritten as

$$\begin{bmatrix} 1 & 0 & -\frac{\mu}{\sqrt{2}} \\ -1 & 0 & -\frac{\mu}{\sqrt{2}} \\ 0 & 1 & -\frac{\mu}{\sqrt{2}} \\ 0 & -1 & -\frac{\mu}{\sqrt{2}} \end{bmatrix} \begin{bmatrix} f_{io} \\ f_{it} \\ f_{in} \end{bmatrix} \le \begin{bmatrix} 0 \\ 0 \\ 0 \end{bmatrix} \tag{20}$$

which gives a conservative but linear set of constraints describing a friction pyramid inscribed within the desired friction cone.

We can rewrite the above equation as

$$S_i f_i \le 0 \tag{21}$$

where $S_i \in R^{\iota}$ is the matrix coefficient of the friction constraints for the ith foot. Considering the boundedness of f_i, we assume that

$$\xi_i^- \le f_i \le \xi_i^+ \tag{22}$$

with the known boundary vectors $\xi_i^- \in R^{\kappa}$ and $\xi_i^+ \in R^{\kappa}$.

The wrench in the global coordinate frame produced by f_i is

$$W_i = G_i f_i \tag{23}$$

where $G_i \in R^{l \times \kappa}$ is the balance matrix for contact i

$$G_i = \begin{bmatrix} n_i & o_i & t_i \\ r_i \times n_i & r_i \times o_i & r_i \times t_i \end{bmatrix} \tag{24}$$

Let $\mathcal{W}_{\mathrm{ext}}$ denote the ''dynamic" external wrench on the biped. For equilibrium, the resultant wrench $\mathcal{W}$ applied by the feet should always conform to

$$\mathcal{W} = \sum_{i=\{l,r\}} W_i = \sum_{i=\{l,r\}} G_i f_i = -\mathcal{W}_{ext} \tag{25}$$

In real-time control of the balance of the biped, $\mathcal{W}_{\mathrm{ext}}$ is sampled at a sequence of instants with sufficiently small intervals. Thus we encounter the dynamic force distribution problem.

Besides the form-closure constraints, to balance any external wrench $\mathcal{W}_{\mathrm{ext}}$ to maintain a stable balance, we consider the quadratic objective function of contact forces. The optimal contact force with holding the balance can be formulated as the following optimization problem with linear and nonlinear constraints

$$\text{minimize} \quad J(f) = \frac{1}{2} f^T Q f + b^T f \tag{26}$$

$$\text{subject to} \quad Gf = \mathcal{W} \tag{27}$$

$$Sf \le C = 0 \tag{28}$$

$$\xi^- \le f \le \xi^+ \tag{29}$$

where $f = [f_l^T, f_r^T]^T \in R^{2\kappa}$, Q is an $2\kappa \times 2\kappa$ symmetric and positive definite matrix, $G = [G_l, G_r] \in R^{l \times 2\kappa}$, $S = [S_l, -S_r] \in R^{\iota \times 2\kappa}$. The above quadratic object function represents the minimum weighted norm of joint torque vectors and minimum norm force when $b = 0$.

From (26) to (29), a unified QP formulation for the external forces and the friction force constraints is developed. Motivated by the work in [33], the neural network was developed to solve online solution of the QP problem for foot force optimization for quadruped robots. In this paper, the primal–dual neural network is adopted to perform the optimization of the reaction forces from the environments.

For constraints (27) and (28), the corresponding dual decision vector is defined as $y \in R^l$. Hence, the primal–dual decision vector u and its upper/lower bounds $u^{\pm}$ are defined, respectively, as

$$u := \begin{bmatrix} f \\ y \\ \beta \end{bmatrix}, u^+ := \begin{bmatrix} \xi^+ \\ +y^+ \\ +y^+ \end{bmatrix}, u^- := \begin{bmatrix} \xi^- \\ +y^+ \\ -y^- \end{bmatrix} \in R^{2\kappa+l+\iota} \quad (30)$$

where for the convenience of hardware implementation or simulation, for any i, the elements $y_i^+ \gg 0$ in y^+ are sufficiently positive to represent $+\infty$. Thus, the convex set Ω made by primal–dual decision vector u is $\Omega = \{u^- \le u \le u^+\}$. Defining the coefficient matrix M and vector p as

$$M = \begin{bmatrix} Q & -G^T & S^T \\ G & 0 & 0 \\ -S^T & 0 & 0 \end{bmatrix} \in R^{(2\kappa+l+\iota)\times(2\kappa+l+\iota)} \quad (31)$$

$$p = \begin{bmatrix} b \\ -\mathcal{W} \\ C \end{bmatrix} \in R^{(2\kappa+l+\iota)} \quad (32)$$

we have the following equivalent result.

Theorem 3.1 [33] (LVI Formulation) *Quadratic program* (26)–(29) *is equivalent to the following linear variational inequalities problem, i.e., to find a vector* $u^* \in \Omega = \{u | u^- \le u \le u^+\}$ *such that*

$$(u - u^*)^T (Mu^* + p) \ge 0, \quad \forall u \in \Omega \quad (33)$$

where coefficients M, p, and $u^{\pm}$ *are defined in* (30) *and* (31)*, respectively.*

It is known that linear variational inequality (33) is equivalent to the following system of piecewise linear equation (also called linear projection equation)

$$P_\Omega(u - (Mu + p)) - u = 0 \quad (34)$$

where $P_\Omega(\cdot)$ is the projection operator onto Ω and defined as $P_\Omega(u) = [P_\Omega(u_1), \cdots, P_\Omega(u_{2\kappa+l+\iota})]^{\mathrm{T}}$ with

$$P_\Omega(u_i) = \begin{cases} u_i^- & if \quad u_i < u_i^- \\ u_i & if \quad u_i^- \le u_i \le u_i^+ \\ u_i^+ & if \quad u_i > u_i^+ \end{cases}, \quad \forall i \in \{1, \ldots, 2\kappa + l + \iota\}.$$

To solve linear projection Eq. (34), we may follow the dual dynamical system design approach [33, 34] to build a dynamical system. However, such a system is not stable due to M being asymmetric. The design experience motivates us to develop the following modified dynamical system to solve (34)

$$\dot{u} = \gamma(I + M^T)\{P_\Omega(u - (Mu + p)) - u\}. \quad (35)$$

where γ is a strictly positive design parameter used to scale the convergence rate of the system.

Theorem 3.2 [33] *Starting from any initial state, the state vector u(t) of primal–dual dynamical system* (35) *is convergent to an equilibrium point* u^**, of which the first n elements constitute the optimal solution* f^* *to the quadratic programming problem in* (26)–(29)*. Moreover, the exponential convergence can be achieved, provided that there exists a constant* $\rho > 0$ *such that* $\|u - P_\Omega(u - (Mu + p))\|_2^2 \ge \rho \|u - u^*\|_2^2$.

Remark 3.1 For the double-support phase, in order to balance the biped under external wrench, and avoid the slipping or slippage and tip-over, we can obtain the ground applied constraints force to a desired value f^*. Therefore, the constraint force errors and $f - f^*$ should be within a small neighborhood of zero, i.e., $\|f - f^*\| \le \varsigma$.

Remark 3.2 The second control objective is to design a position control such that the tracking error of q_1 and $\dot{q}_1$ from their respective desired trajectories q_1^d and $\dot{q}_1^d$ are within a small neighborhood of zero, i.e., $\|q_1 - q_1^d\| \le \varepsilon_1$, and $\|\dot{q}_1 - \dot{q}_1^d\| \le \varepsilon_2$. The desired reference trajectory q_1^d is assumed to be bounded and uniformly continuous, and has bounded and uniformly continuous derivatives up to the second order.

In summary, the control structure is shown in Fig. 2.

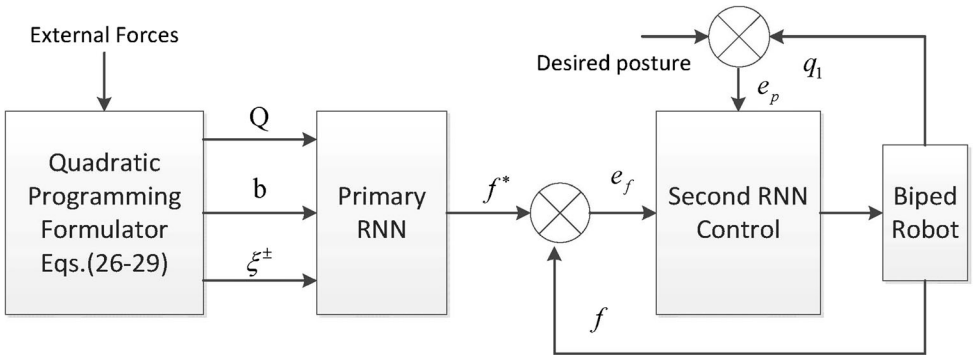

Fig. 2 The control structure

4 Hybrid motion/force control using RNN

4.1 Recurrent neural network

A three-layer RNN shown in [38] comprises an input layer, a hidden layer with a feedback unit, and an output layer. The Gaussian function is adopted as the activation function in the hidden layer due to its continuous and differential characteristics. The mapping of the RNN is according to the following equation

$$z(N) = \sum_{i=1}^{n} w_k \Theta_k(\|x_i(N) - v_{ik}\|, \sigma_{ik}, r_k, \Theta_k(N-1)) \quad (36)$$

where $x = x_i$, $i = 1, 2, \ldots, m$ are the input variables; z is the output variable; N is the number of iterations; w_k represents the connective weights between the hidden layer and the output layer; Θ_k represents the output of the kth neurons in the hidden layer; v_{ik} and σ_{ik} are the center and width of the Gaussian function; r_k is the internal feedback gain; and $\|\cdot\|$ denotes the Euclidean norm. The weight can be represented as

$$\text{net}_k(N) = \sum_{i=1}^{m} \delta_{ik}^2 [x_i(N) + \Theta_k(N-1) r_k - v_{ik}]^2 \quad (37)$$

or

$$\text{net}_k(N) = \sum_{i=1}^{m} \frac{[x_i(N) + \Theta_k(N-1) r_k - v_{ik}]^2}{\sigma_{ik}^2} \quad (38)$$

and

$$\Theta_k(N) = \exp(-\text{net}_k(N)) \quad (39)$$

where $\delta_{ik} = 1/\sigma_{ik}$ is the inverse radius of the Gaussian function. Define vectors δ, v and r to be the collection of all parameters in the hidden layer in RNN as

$$\delta = [\delta_{11}, \ldots, \delta_{m1}, \delta_{12}, \ldots, \delta_{m2}, \ldots, \delta_{1n}, \ldots, \delta_{mn}]^T \quad (40)$$

$$v = [v_{11}, \ldots, v_{m1}, v_{12}, \ldots, v_{m2}, \ldots, v_{1n}, \ldots, v_{mn}]^T \quad (41)$$

$$r = [r_1, \ldots, r_n]^T \quad (42)$$

Then the output of the RNN can be represented in a vector form as

$$y(x, \delta, v, r, W) = W^T \Theta(x, \delta, v, r) \quad (43)$$

where $W = [w_1, \ldots, w_n]^T$ and $\Theta = [\Theta_1, \ldots, \Theta_n]^T$. It has been proven in [26] that there exists an RNN of (43) such that it can uniformly approximate a nonlinear, even time-varying function.

The approximation error of the RNN output is denoted as

$$\tilde{y} = y - \hat{y} = W^{*T} \Theta(x, \delta^*, v^*, r^*) - \hat{W}^T \Theta(x, \hat{\delta}, \hat{v}, \hat{r}) + \varepsilon \quad (44)$$

where ε is a minimum reconstructed error due to the insufficient number of neurons at the hidden layer; δ^*, v^* and r^* are optimal parameters of δ, v and r, and $\hat{\delta}$, $\hat{v}$ and $\hat{r}$ are the estimates of the optimal parameters δ^*, v^* and r^*.

Assumption 4.1 The ideal RNN vectors W^*, δ^*, v^*, r^* and the RNN approximation error are bounded over the compact set, i.e.,

$$\|W^*\| \le w_m, \|\delta^*\| \le \delta_m, \|v^*\| \le v_m, \|r^*\| \le r_m, |\epsilon(x)| \le \epsilon^*$$

$\forall x \in \Omega_x$ with w_m, δ_m, v_m, r_m and ϵ^* being unknown positive constants.

Remark 4.1 The optimal weight vector W^*, δ^*, v^*, r^* in (43) is an ''artificial'' quantity required only for analytical purposes. Typically, W^*, δ^*, v^*, r^* are chosen as the values that minimize $\epsilon(x)$ for all $x \in \Omega_x \subset \mathbb{R}^{n_i}$, i.e.,

$$(W^*, \delta^*, v^*, r^*) := \arg \min_{W, \delta, v, r} \{ \sup_{x \in \Omega_x} |y - W^T \Theta(x, \delta, v, r)| \}$$

Remark 4.2 The approximation error $\epsilon(x)$ is a critical quantity and can be reduced by increasing the number of neurons in the hidden layer. According to the universal approximation theorem, it can be made as small as possible if the number of neurons is sufficiently large [39, 40].

From the above analysis, we see that the system uncertainties are converted to the estimation of unknown parameters W^*, δ^*, v^*, r^* and unknown bounds ϵ^*.

As the ideal vectors/constants W^*, δ^*, v^*, r^* and ϵ^* are usually unknown, we use their estimates $\hat{W}$, $\hat{\delta}$, $\hat{v}$, $\hat{r}$ and $\hat{\epsilon}$ instead. The following lemma gives the properties of the approximation errors $\hat{W}^T \Theta(x, \hat{\delta}, \hat{v}, \hat{r}) - W^{*T} \Theta(x, \delta^*, v^*, r^*)$. The definition of induced norm of matrices is given here first.

The approximation error can be expressed as

$$\begin{aligned} \tilde{y} &= \hat{W}^T \Theta(x, \hat{\delta}, \hat{v}, \hat{r}) - W^{*T} \Theta(x, \delta^*, v^*, r^*) \\ &= W^{*T} \tilde{\Theta} + \tilde{W}^T \hat{\Theta} + d_u \end{aligned} \quad (45)$$

where $\hat{\Theta} = \Theta(x, \hat{\delta}, \hat{v}, \hat{r})$, $\tilde{W} = \hat{W} - W^*$, $\tilde{\delta} = \hat{\delta} - \delta^*$, $\tilde{v} = \hat{v} - v^*$ and $\tilde{r} = \hat{r} - r^*$ are defined as approximation errors, and The expansion of $\tilde{\Theta}$ in Taylor series is obtained as follows

$$\tilde{\Theta} = \begin{bmatrix} \tilde{\Theta}_1 \\ \tilde{\Theta}_2 \\ \vdots \\ \tilde{\Theta}_k \end{bmatrix} = \begin{bmatrix} \frac{\partial \Theta_1}{\partial \delta} \\ \frac{\partial \Theta_2}{\partial \delta} \\ \vdots \\ \frac{\partial \Theta_k}{\partial \delta} \end{bmatrix}^T \Big|_{\delta=\hat{\delta}} (\delta^* - \delta) + \begin{bmatrix} \frac{\partial \Theta_1}{\partial v} \\ \frac{\partial \Theta_2}{\partial v} \\ \vdots \\ \frac{\partial \Theta_k}{\partial v} \end{bmatrix}^T \Big|_{v=\hat{v}} (v^* - v) + \begin{bmatrix} \frac{\partial \Theta_1}{\partial r} \\ \frac{\partial \Theta_2}{\partial r} \\ \vdots \\ \frac{\partial \Theta_k}{\partial r} \end{bmatrix}^T \Big|_{r=\hat{r}} (r^* - r) + N \quad (46)$$

$$= \Theta_\delta^T \tilde{\delta} + \Theta_v^T \tilde{v} + \Theta_r^T \tilde{r} + N$$

where $\Theta_\delta = \left[\frac{\partial \Theta_1}{\partial \delta} \quad \frac{\partial \Theta_2}{\partial \delta} \quad \cdots \quad \frac{\partial \Theta_k}{\partial \delta} \right] \Big|_{\delta=\hat{\delta}} \in R^{j \times k}$, $\Theta_v = \left[\frac{\partial \Theta_1}{\partial v} \quad \frac{\partial \Theta_2}{\partial v} \quad \cdots \quad \frac{\partial \Theta_k}{\partial v} \right] \Big|_{v=\hat{v}} \in R^{j \times k}$, $\Theta_v = \left[\frac{\partial \Theta_1}{\partial r} \quad \frac{\partial \Theta_2}{\partial r} \quad \cdots \quad \frac{\partial \Theta_k}{\partial r} \right] \Big|_{r=\hat{r}} \in R^{j \times k}$, and N is a vector of higher-order terms and assumed to be bounded by a positive constant. Substituting (46) into (45), one obtains [41]

$$\begin{aligned} &\hat{W}^T \Theta(x, \hat{\delta}, \hat{v}, \hat{r}) - W^{*^T} \Theta(x, \delta^*, v^*, r^*) = (\tilde{W} + W^*)^T \\ &\Theta(x, \hat{\delta}, \hat{v}, \hat{r}) - W^{*^T} [\Theta(x, \hat{\delta}, \hat{v}, \hat{r}) - \Theta_\delta^T \tilde{\delta} - \Theta_v^T \tilde{v} - \Theta_r^T \tilde{r} \\ &+ O(x, \tilde{\delta}, \tilde{v}, \tilde{r})] = \tilde{W}^T \hat{\Theta} + (\hat{W} - \tilde{W})^T \hat{\Theta}_\delta \tilde{\delta} + (\hat{W} - \tilde{W})^T \\ &\Theta_v^T \tilde{v} + (\hat{W} - \tilde{W})^T \Theta_r^T \tilde{r} - W^{*^T} O(x, \tilde{\delta}, \tilde{v}, \tilde{r}) \\ &= \tilde{W}^T \hat{\Theta} + \hat{W}^T \Theta_\delta^T \tilde{\delta} - \tilde{W}^T \Theta_\delta^T (\hat{\delta} - \delta^*) + \hat{W}^T \Theta_v^T \tilde{v} \\ &- \tilde{W}^T \Theta_v^T (\hat{v} - v^*) + \hat{W}^T \Theta_r^T \tilde{r} - \tilde{W}^T \Theta_r^T (\hat{r} - r^*) \\ &- W^{*^T} O(x, \tilde{\delta}, \tilde{v}, \tilde{r}) = \tilde{W}^T (\hat{\Theta} - \Theta_\delta^T \hat{\delta} - \Theta_v^T \hat{v} - \Theta_r^T \hat{r}) \\ &+ \hat{W}^T (\Theta_\delta^T \tilde{\delta} + \Theta_v^T \tilde{v} + \Theta_r^T \tilde{r}) + \Delta \end{aligned} \quad (47)$$

where $\Delta = W^{*T}(\Theta_\delta^T \delta^* + \Theta_v^T v^* + \Theta_r^T r^* + O) - \hat{W}^T(\Theta_\delta^T \delta^* + \Theta_v^T v^* + \Theta_r^T r^*)$ is defined as the lumped uncertainty.

4.2 Hybrid motion/force control

Inspired by pure-motion tracking, some notations are defined as

$$e_1 = q_1 - q_1^d \quad (48)$$

$$r = \dot{e}_1 + \Lambda e_1 \quad (49)$$

$$\dot{q}_1^r = \dot{q}_1^d - \Lambda e_1 \quad (50)$$

where $\Lambda \in R^{(n-m)\times(n-m)}$ is a positive diagonal matrix.

If the system satisfies $\lim_{t\to\infty} = 0$, then position and velocity tracking errors e_1 and $\dot{e}_1$ exponentially converge to zero. In other words, the error signal r is an error measurement deviating from the stable subspace $\{e_1, \dot{e}_1 \in R^{n-m} | r = 0\}$. The motion tracking problem is, therefore, transformed to the problem of stabilizing r. On the other hand, a force-error and its filter are accordingly defined as

$$e_f = f - f^* \quad (51)$$

$$\dot{\alpha} = -\rho_1 \alpha - \rho_2^{-1}(1 + k_f) J^T e_f \quad (52)$$

where $\rho_1, \rho_2 > 0, k_f > 0$ are design parameters, $e_f = f - f^*$. Then, the reduced-state-based scheme is to drive the motion trajectory into the stable subspace, while the contact force is separately controlled, maintaining a zero e_f.

Combine $r \in R^{n-m}$ to form the following new hybrid variables

$$\sigma = Hr + \alpha \quad (53)$$

$$v = H\dot{q}_1^r - \alpha \quad (54)$$

From (50), (53), and (54), we have

$$\sigma + v = H\dot{q}_1 \quad (55)$$

The time derivatives of v and σ are given by

$$\dot{v} = \dot{H}\dot{q}_1^r + Hq_1^r - \dot{\alpha} \quad (56)$$

$$\dot{\sigma} = \dot{H}\dot{q}_1^r + Hq_1^r + \dot{\alpha} \quad (57)$$

From the dynamic Eq. (15) together with (55) and (57), we have

$$M(q)\dot{\sigma} + \mu = \tau + J^T f \quad (58)$$

where $\mu = M(q)\dot{v} + C(q, \dot{q})(v + \sigma) + G(q)$. We can rewrite Eq. (58) as

$$M(q)\dot{\sigma} = \tau - \mu + J^T f \quad (59)$$

Consider the control law

$$\tau = \hat{M}(q)\dot{v} + \hat{C}(q, \dot{q})v + \hat{G}(q) - K_\sigma \sigma - J^T f^* + k_f J^T e_f - K_s \mathrm{sgn}(\sigma) - \hat{\Delta} \quad (60)$$

where matrix $K_\sigma > 0$, constant $k_f > 0$, matrix $K_s = \mathrm{diag}\{k_{sii}\}$ with $k_{sii} \geq |E_i|$ and E_i is the element of vector E (defined later), $e_f = f - f^*$, and $\hat{\Delta}$ is an on-line estimated value of the lumped uncertainty Δ, and $\tilde{\Delta} = \hat{\Delta} - \Delta$, $\hat{M}(q)$, $\hat{C}(q, \dot{q})$, and $\hat{G}(q)$ are the estimates of $M(q)$, $C(q, \dot{q})$ and $G(q)$, respectively, the elements of which, i.e., $m_{ij}(q)$, $c_{ij}(q, \dot{q})$, and $g_i(q)$ can be expressed by RNN as

$$m_{ij}(q) = W_{m_{ij}}^{*^T} \Theta(q, \delta_{m_{ij}}^*, v_{m_{ij}}^*, r_{m_{ij}}^*) + \epsilon_{m_{ij}}(q) \quad (61)$$

$$c_{ij}(q, \dot{q}) = W_{c_{ij}}^{*^T} \Theta(q, \dot{q}, \delta_{c_{ij}}^*, v_{c_{ij}}^*, r_{c_{ij}}^*) + \epsilon_{c_{ij}}(q, \dot{q}) \quad (62)$$

$$g_i(q) = W_{g_i}^{*^T} \Theta(q, \delta_{g_i}^*, v_{g_i}^*, r_{g_i}^*) + \epsilon_{g_i}(q) \quad (63)$$

where $W^*_{m_{ij}}$, $W^*_{c_{ij}}$, $W^*_{g_i}$ are ideal constant weight vectors, $\delta^*_{m_{ij}}$, $\delta^*_{c_{ij}}$, $\delta^*_{g_i}$ are the ideal vectors, $v^*_{m_{ij}}$, $v^*_{c_{ij}}$, $v^*_{g_i}$ are the ideal vectors, $r^*_{m_{ij}}$,$r^*_{c_{ij}}$, $r^*_{g_i}$ are the ideal vectors, and $\epsilon_{m_{ij}}(q)$, $\epsilon_{c_{ij}}(q,\dot{q})$, $\epsilon_{g_i}(q)$ are the approximation errors.

Using the GL matrix (denoted by "$\{\bigstar\}$") and operator (denoted by "$\cdot$") introduced in [37, 42], the function emulators (61)–(63) can be collectively expressed as

$$M(q) = [\{W^*_M\}^T \cdot \{\Theta_M\}] + E_M \tag{64}$$

$$C(q,\dot{q}) = [\{W^*_C\}^T \cdot \{\Theta_C\}] + E_C \tag{65}$$

$$G(q) = [\{W^*_G\}^T \cdot \{\Theta_G\}] + E_G \tag{66}$$

where $[\{W^*_M\}, \{\Theta_M\}]$, $[\{\mathrm{W}^*_C\}, \{\Theta_C\}]$ and $[\{\mathrm{W}^*_G\}, \{\Theta_G\}]$ are the desired weights and basis function GL matrices pairs of the RNN emulation of $M(q)$,$C(q,\dot{q})$ and $G(q)$ respectively; and E_M, E_C, E_G are the collective RNN reconstruction errors, respectively.

The estimates $\hat{M}(q)$, $\hat{C}(q,\dot{q})$, $\hat{G}(q)$, can be accordingly expressed as

$$\hat{M}(q) = [\{\hat{W}_M\}^T \cdot \{\hat{\Theta}_M\}] \tag{67}$$

$$\hat{C}(q,\dot{q}) = [\{\{\hat{W}_C\}^T \cdot \{\hat{\Theta}_C\}] \tag{68}$$

$$\hat{G}(q) = [\{\{\hat{W}_G\}^T \cdot \{\hat{\Theta}_G\}] \tag{69}$$

Substituting (60) and (67)–(69) into the dynamic Eq. (58) yields the closed-loop system error equation as

$$\begin{aligned} M\dot{\sigma} + C\sigma = {} & ([\{\hat{W}\}^T \cdot \{\Theta\}] - [\{\mathrm{W}^*\}^{\mathrm{T}} \cdot \{\Theta\}]) - K_\sigma\sigma \\ & + J^T(1+k_f)e_f - E - K_s\mathrm{sgn}(\sigma) - \hat{\Delta} \end{aligned} \tag{70}$$

where

$$\{\hat{W}\}^T = [\{\hat{W}_M\}^T, \{\hat{W}_C\}^T, \{\hat{W}_G\}^T]^T$$

$$\{\hat{\Theta}\} = [\{\hat{\Theta}_M\}\dot{v}, \{\hat{\Theta}_C\}v, \{\hat{\Theta}_G\}]^T$$

$$\{\mathrm{W}^*\}^T = [\{\mathrm{W}^*_M\}^T, \{\mathrm{W}^*_C\}^T, \{\mathrm{W}^*_G\}^T]^T$$

$$\{\Theta\} = [\{\Theta_M\}\dot{v}, \{\Theta_C\}v, \{\Theta_G\}]^T$$

where $E = E_M\dot{v} + E_C v + E_G$.

Theorem 4.1 *Consider the system described by dynamic Eq. (4) and m independent constraints (9). If the control law is chosen by (60), and the parameter adaptation laws are chosen by*

$$\dot{\hat{W}} = -\Gamma_w \cdot \{\hat{\Theta} - \Theta^T_\delta\hat{\delta} - \Theta^T_v\hat{v} - \Theta^T_r\hat{r}\}\sigma \tag{71}$$

$$\dot{\hat{\delta}} = -\Gamma_\delta[\hat{W} \cdot \Theta_\delta]\sigma \tag{72}$$

$$\dot{\hat{v}} = -\Gamma_v[\hat{W} \cdot \Theta_v]\sigma \tag{73}$$

$$\dot{\hat{r}} = -\Gamma_r[\hat{W} \cdot \Theta_r]\sigma \tag{74}$$

$$\dot{\hat{\Delta}} = \Gamma_h\sigma \tag{75}$$

where matrices Γ_w, Γ_δ, Γ_r, Γ_v, Γ_h are symmetric positive definite, then, the signals e_1 and $\dot{e}_1$ asymptotically converge to zero, and all the other closed-loop signals are semi-globally uniformly ultimately bounded.

Proof The time derivative of $\frac{1}{2}\sigma^T M\sigma$ along (70) is

$$\begin{aligned} \sigma^T M^T\dot{\sigma} = {} & -\sigma^T K_\sigma\sigma - \sigma^T E - \sigma^T K_s\mathrm{sgn}(\sigma) - \sigma^T\hat{\Delta} \\ & + \sigma^T J^T(1+k_f)e_f - \sigma^T C\sigma \\ & + \sigma^T([\{\hat{W}\}^T \cdot \{\hat{\Theta}\}] - [\{W^*\}^T \cdot \{\Theta\}]) \end{aligned} \tag{76}$$

Consider the Lyapunov function candidate

$$\begin{aligned} V = {} & \frac{1}{2}\sigma^T M\sigma + \tilde{\mathrm{W}}^T\Gamma_w^{-1}\tilde{\mathrm{W}} + \frac{1}{2}\tilde{\delta}^T\Gamma_\delta^{-1}\tilde{\delta} + \frac{1}{2}\tilde{v}^T\Gamma_v^{-1}\tilde{v} + \frac{1}{2}\tilde{r}^T\Gamma_r^{-1}\tilde{r} \\ & + \frac{1}{2}\tilde{\Delta}^T\Gamma_h^{-1}\tilde{\Delta} + \frac{1}{2}\rho_2\alpha^T\alpha \end{aligned} \tag{77}$$

with $\tilde{x} = \hat{x} - x^*$.

The time derivative of V is given by

$$\begin{aligned} \dot{V} = {} & \sigma^T M\dot{\sigma} + \frac{1}{2}\sigma^T\dot{M}\sigma + \tilde{W}^T\Gamma_w^{-1}\dot{\hat{W}} + \tilde{\delta}^T\Gamma_\delta^{-1}\dot{\tilde{\delta}} + \tilde{v}^T\Gamma_v^{-1}\dot{\tilde{v}} \\ & + \tilde{r}^T\Gamma_r^{-1}\dot{\tilde{r}} + \tilde{\Delta}^T\Gamma_h^{-1}\dot{\tilde{\Delta}} \le \frac{1}{2}\sigma^T\dot{M}\sigma - \sigma^T C\sigma - \sigma^T K_\sigma\sigma \\ & - \sigma^T E - \sigma^T K_s\mathrm{sgn}(\sigma) - \sigma^T\hat{\Delta} + \sigma^T J^T(1+k_f)e_f \\ & + \sigma^T([\{\hat{W}\}^T \cdot \{\hat{\Theta}\}] - [\{W^*\}^T \cdot \{\Theta\}]) \\ & + \tilde{W}^T\Gamma_w^{-1}\dot{\hat{W}} + \tilde{\delta}^T\Gamma_\delta^{-1}\dot{\tilde{\delta}} + \tilde{v}^T\Gamma_v^{-1}\dot{\tilde{v}} + \tilde{r}^T\Gamma_r^{-1}\dot{\tilde{r}} \\ & + \tilde{\Delta}^T\Gamma_h^{-1}\dot{\tilde{\Delta}} + \rho_2\alpha^T\dot{\alpha} \end{aligned} \tag{78}$$

As matrix $\dot{M} - 2C$ is skew-symmetric, $\sigma^T(\dot{M} - 2C)\sigma = 0$, $\forall x \neq 0$. Integrating (47) into (78), we have

$$\begin{aligned} \dot{V} \le {} & -\sigma^T K_\sigma\sigma - \sigma^T E - \sigma^T K_s\mathrm{sgn}(\sigma) - \sigma^T\hat{\Delta} + \sigma^T J^T(1+k_f)e_f \\ & + \sigma^T\Big([\{\tilde{W}^T\} \cdot \{\hat{\Theta} - \Theta^T_\delta\hat{\delta} - \Theta^T_v\hat{v} - \Theta^T_r\hat{r}\}] + [\{\hat{W}^T\} \cdot \\ & \Big\{\Theta^T_\delta\tilde{\delta} + \Theta^T_v\tilde{v} + \Theta^T_r\tilde{r}\}] + \Delta\Big) + \tilde{W}^T\Gamma_w^{-1}\dot{\hat{W}} + \tilde{\delta}^T\Gamma_\delta^{-1}\dot{\tilde{\delta}} \\ & + \tilde{v}^T\Gamma_v^{-1}\dot{\tilde{v}} + \tilde{r}^T\Gamma_r^{-1}\dot{\tilde{r}} + \tilde{\Delta}^T\Gamma_h^{-1}\dot{\tilde{\Delta}} + \rho_2\alpha^T\dot{\alpha} \end{aligned} \tag{79}$$

Substituting the weight vectors updating laws (71–75) into (79) yields

$$\begin{aligned} \dot{V} \le {} & -\sigma^T K_\sigma\sigma - \sigma^T E - \sigma^T K_s\mathrm{sgn}(\sigma) \\ & + \sigma^T J^T(1+k_f)e_f + \rho_2\alpha^T\dot{\alpha} \end{aligned} \tag{80}$$

Noting that $k_{sii} \ge |E_i| > 0$, it is obvious that $[-\sigma^T E - \sigma^T K_s\mathrm{sgn}(\sigma)] \le 0$. In addition, from (52), we know that $\dot{\alpha} = -\rho_1\alpha - \rho_2^{-1}(1+k_f)J^T e_f$ and from (53), $\sigma^T = r^{T\text{-}}H^T + \alpha^T$. Thus, we have

$$\sigma^T J^T(1+k_f)e_f + \rho_2\alpha^T\dot{\alpha} = -\rho_1\rho_2\alpha^T\alpha + r^T H^T J^T(1+k_f)e_f \tag{81}$$

Noting $H^T J^T = 0$ from (11) and (26), we then have

$$\dot{V} \leq -\sigma^T K_\sigma \sigma - \rho_1\rho_2\alpha^T\alpha \leq 0 \tag{82}$$

As $V \geq 0$ and $\dot{V} \leq 0$, $V \in L_\infty$. From the definition of V, it follows that σ, $v \in L_\infty^n$.

Integrating both sides of (82), we have

$$\int_0^t \sigma^T K_\sigma \sigma \leq V(0) - V(t) \leq V(0) \tag{83}$$

Hence $\sigma \in L_2^n$. From (53), we have $r = (H^T H)^{-1} H^T(\sigma - \alpha)$, hence $r \in L_\infty^{n-m}$ since H is bounded. From Lemma 2.1, it can be concluded that $e_1, \dot{e}_1 \in L_\infty^{n-m}$. From (53–56), we have

$$\begin{aligned}\hat{M}\dot{v} + \hat{C}v + \hat{G} &= \hat{M}(\dot{H}\dot{q}_1^r + Hq_1^r - \dot{\alpha}) + \hat{C}(H\dot{q}_1^r - \alpha) + \hat{G} \\ &= \hat{M}(\dot{H}\dot{q}_1^r + Hq_1^r) + \hat{C}H\dot{q}_1^r + \hat{G} \\ &\quad + (\rho_1\hat{M} - \hat{C})\alpha + \rho_2^{-1}(1+k_f)\hat{M}J^T e_f \end{aligned} \tag{84}$$

From (48–50), it is known that

$$\dot{q} = H\dot{q}_1^r + Hr \tag{85}$$

$$q = \dot{H}\dot{q}_1^r + Hq_1^r + \dot{H}r + H\dot{r} \tag{86}$$

Replacing τ by (60) in dynamic Eq. (15), and Eqs. (84–86), the closed-loop system becomes

$$\begin{aligned}&M\dot{H}r + MH\dot{r} + CHr - (\hat{M} - M)(\dot{H}\dot{q}_1^r + Hq_1^r) \\ &\quad - (\hat{C} - C)H\dot{q}_1^r - (\hat{G} - G) + (\hat{C} - \rho_1\hat{M})\alpha + K_\sigma\sigma \\ &\quad + K_s\mathrm{sgn}(\sigma) = (\rho_2^{-1}(1+k_f)\hat{M} + I_n)J^T e_f \end{aligned} \tag{87}$$

Invoking (64–66) and (67–69), Eq. (87) then becomes

$$\begin{aligned}&M\dot{H}r + MH\dot{r} + CHr - ([\{\hat{W}_M\}^T \cdot \{\hat{\Theta}_M\}] - [\{W_M^*\}^T \cdot \\ &\quad \{\Theta_M\}])(\dot{H}\dot{q}_1^r + Hq_1^r) - ([\{\hat{W}_C\}^T \cdot \{\hat{\Theta}_C\}] - [\{W_C^*\}^T \cdot \\ &\quad \{\Theta_C\}])H\dot{q}_1^r - ([\{\hat{W}_G\}^T \cdot \{\hat{\Theta}_G\}] - [\{W_G^*\}^T \cdot \{\Theta_G\}]) \\ &\quad + (\hat{C} - \rho_1\hat{M})\alpha + K_\sigma\sigma + K_s\mathrm{sgn}(\sigma) + E_M(\dot{H}\dot{q}_1^r + Hq_1^r) \\ &\quad + E_C H\dot{q}_1^r + E_G = (\rho_3^{-1}(1+k_f)\hat{M} + I_n)J^T e_f \end{aligned} \tag{88}$$

Since $M(q)$ is nonsingular, multiplying $H(q)M^{-1}(q)$ on both sides of (88) yields

$$\begin{aligned}&H\dot{H}r + HM^{-1}[CHr - ([\{\hat{W}_M\}^T \cdot \{\hat{\Theta}_M\}] - [\{W_M^*\}^T \cdot \{\Theta_M\}]) \\ &(\dot{H}\dot{q}_1^r + Hq_1^r) - ([\{\hat{W}_C\}^T \cdot \{\hat{\Theta}_C\}] - [\{W_C^*\}^T \cdot \{\Theta_C\}])H\dot{q}_1^r \\ &\quad - ([\{\hat{W}_G\}^T \cdot \{\hat{\widehat{\Theta}}_G\}] - [\{W_G^*\}^T \cdot \{\Theta_G\}]) + (\hat{C} - \rho_1\hat{M})\alpha \\ &\quad + K_\sigma\sigma + K_s\mathrm{sgn}(\sigma) + E_M(\dot{H}\dot{q}_1^r + Hq_1^r) + E_C H\dot{q}_1^r + E_G] \\ &\quad = HM^{-1}(\rho_3^{-1}(1+k_f)\hat{M} + I_n)J^T e_f \end{aligned} \tag{89}$$

Since we have established that $e_1, \dot{e}_1 \in L_\infty^{n-m}$, from (50), it can be concluded that $\dot{q}_1^r, q_1^r \in L_\infty^{n-m}$. As r is shown to be bounded, so is $\dot{q}_1$ from (50). Hence, $\dot{q}(t) = H\dot{q}_1 \in L_\infty^n$. It follows that $M(q), \hat{M}(q), C(q,\dot{q}), \hat{C}(q,\dot{q}) \in L_\infty^{n\times n}$, and $G(q), \hat{G}(q) \in L_\infty^n$. Thus, the left-hand side of (89) is bounded. In fact, ρ_3 can be properly chosen to keep $(\rho_3^{-1}(1+k_f)\hat{M} + I_n)$ on the right-hand side of (89) from being singular. Hence, we have $e_f \in L_\infty^{n-m}$. As f^* is bounded, so are e_f and τ.

As $\lambda \in L_\infty^{n-m}$ and $\alpha \in L_\infty^m$, from Eq. (52), it is obvious that $\dot{\alpha} \in L_\infty^m$. Thus, from (56), we have $\dot{v} \in L_\infty^n$. Since $\dot{q}_1, q_1 \in L_\infty^{n-m}$ have been established before, we can conclude from (57) that $\dot{\sigma} \in L_\infty^n$. Now, with $\sigma, \alpha \in L_2^n$, $\dot{\sigma}, \dot{\alpha} \in L_\infty^n$, according to Lemma 2.2, we can conclude that σ and μ asymptotically converge to zero. Hence, from (53), it can be concluded that $r \to 0$ as $t \to \infty$. According to Lemma 2.2, we can also obtain $e_1, \dot{e}_1 \to 0$ as $t \to \infty$.

Since $\dot{q}, q \in L_\infty^n$, q and $\dot{q}$ are uniformly continuous. Therefore, from Property 2.1, we can conclude that matrices $M(q)$, $C(q,\dot{q})$, $G(q)$, $H(q)$,$J(q)$, $\hat{M}(q)$, $\hat{C}(q,\dot{q})$, and $\hat{G}(q)$ are uniformly continuous.

5 Simulations and experiments

5.1 Simulations

In this section, to show the effectiveness of the proposed approach, we first present simulation results for dynamic balance optimization and control.

Consider a 12-DOF biped robot shown in Fig. 3, which is modeled using ADAMS and consists of a torso, and a pair of legs composed of six links. The left and right legs are numbered as Leg 1 and Leg 2, respectively. The height of the biped is 1.2 m, the length of the lower limbs is 460 mm, and the height of the foot is 90 mm.

Both the balancing optimization and the motion/force tracking under perturbing external forces are evaluated in Fig. 3. In the simulations, diverse external forces with different directions and acting points are considered. Three cases (Case 1: $f_{\text{ext}} = 50\ N$, $\alpha = 0^o$, $d = 1.0$ m; Case 2: $f_{\text{ext}} = 50\ N$, $\alpha = 30^o$, $d = 1.0$ m; Case 3: $f_{\text{ext}} = 50\ N$, $\alpha = 0^o$, $d = 1.2$ m) are illustrated in Fig. 3. We can obtain the corresponding matrices in (26)–(29) as

$$G = \begin{bmatrix} 1 & 0 & 0 & -1 & 0 & 0 \\ 0 & 1 & 0 & 0 & 1 & 0 \\ 0 & 0 & 1 & 0 & 0 & 1 \\ 0 & 0 & l & 0 & 0 & l \end{bmatrix}$$

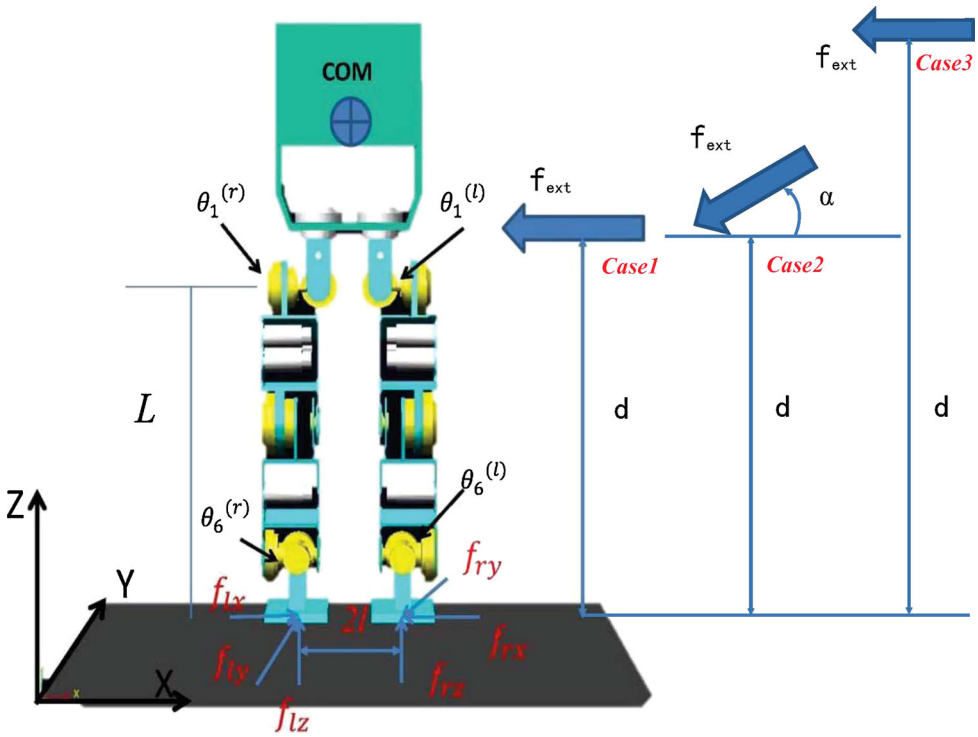

Fig. 3 Diverse external forces in three Cases are applied in the simulations

$$S = \begin{bmatrix} 1 & 0 & -\frac{\mu}{\sqrt{2}} \\ -1 & 0 & -\frac{\mu}{\sqrt{2}} \\ 0 & 1 & -\frac{\mu}{\sqrt{2}} \\ 0 & -1 & -\frac{\mu}{\sqrt{2}} \end{bmatrix}$$

$$f = [f_{lx}, f_{ly}, f_{lz}, f_{rx}, f_{ry}, f_{rz}]^T$$

$$W = [0, f_{ext}cos(\alpha), G, f_{ext}cos(\alpha)d]^T$$

We assume $-20\ N \le f_{lx} \le 20\ N$, $-20\ N \le f_{rx} \le 20\ N$, $-20\ N \le f_{ly} \le 20\ N$, $-20\ N \le f_{ry} \le 20\ N$, therefore, $\zeta^+ = \zeta^- = [20, \ldots, 20]^T$. We choose $Q = \text{diag}[1.0]$, $b = 0$. The friction coefficient of each foot is $\mu = 0.6$.

Under the perturbing external force, both feet are on the ground and the body sways to the right, to the left and then returns to its original position. Because the motion is constrained on the lateral plane, only four joints θ_6^l, θ_1^l, θ_1^r and θ_6^r are actuated and the other eight joints are locked by axis brakes. Figure 3 shows the simplified biped model from the frontal plane. Let the state X and the control U be represented as

$$X = [x_1, x_2, x_3, x_4]^T = [\theta_6^l, \theta_1^l, \theta_1^r, \theta_6^r]^T$$

$$U = [u_1, u_2, u_3, u_4]^T = [\tau_6^l, \tau_1^l, \tau_1^r, \tau_6^r]^T$$

The constraints can be denoted by

$$\begin{bmatrix} L\cos(x_1) \\ L\sin(x_1) \\ x_1 \end{bmatrix} - \begin{bmatrix} 2l + L\cos(x_4) + l\sin(x_3 + x_4) \\ L\sin(x_4) - l\cos(x_3 + x_4) \\ x_3 + x_4 - x_2 \end{bmatrix} = 0$$

where L is the length of the leg and l is half the width of the body. Let x_1 and x_2 be defined by

$$X = [X_1, X_2]^T, X_1 = [x_1], X_2 = [x_2, x_3, x_4]^T \quad (90)$$

It is easy to have $\dot{X}_2 = [-1, -1, 1]^T \dot{X}_1$.The dynamic equation of motion involving only X_1 becomes

$$M\ddot{X}_1 + G = u_1 - u_2 - u_3 + u_4 \quad (91)$$

where $M = 2(I_2 + I_4) + 4(m_2 + m_3)d_2^2 + m_4L^2$, and $G = -(m_2 + m_3 + m_4)gL \sin(x_1)$.and m_4 is the mass of the body; m_3 is the mass of the upper leg; m_2 is the length of the lower leg; I_2 is the inertial moment of the lower leg in the frontal plane; and I_3 is the inertial moment of the upper leg in the frontal plane; and g is the gravity term. For the M and G, 35 nodes are chosen for each variable, with the variances $\sigma_M = \sigma_G = \sigma_t = 2.0$; moreover, the centers are evenly distributed to span the input space $[-1.0, 1.0]$. The weight matrices Φ_M and Φ_G are all initialized to zero. The gains for the controller are chosen as $K_\sigma = \text{diag}[50]$, $\Lambda = \text{diag}[20]$, $K_f = 800$ and $K_s = 10.0$, $\hat{\Delta} = 0$, $\rho_1 = \rho_2 = 0.5$. The adaptation algorithm as given in (71)–(75) is activated with $\Gamma_w = \Gamma_\delta = \Gamma_v = \Gamma_r = \Gamma_h = \text{diag}(0.5)$.

The simulation results for the biped can be found in Figs. 4, 5, 6, 7, 8, 9, 10, 11, 12 and 13. The ground reaction forces of the legs are shown in Figs. 4, 5, 6, 7, 8 and 9. In Case 2, the magnitude of f_z is bigger than that in Case 1 because of the change of the direction of the external force. In Case 3, the difference between ground reaction forces for the two legs is bigger than that in Case 1 because the acting point of the external force is higher. However, all the simulation results show that the force tracking errors tend to the origins in cases of diverse external forces with different directions and acting points.

The input torques for the joints in all three cases can be found in Figs. 10 and 11. The joint velocities for both legs

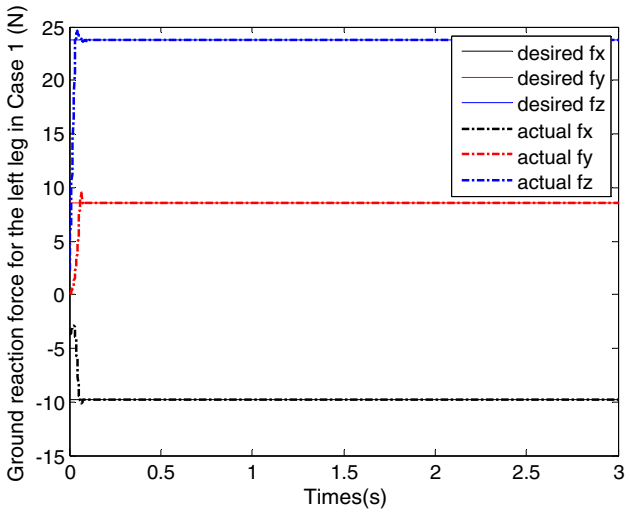

Fig. 4 Ground reaction force for the left leg in Case 1

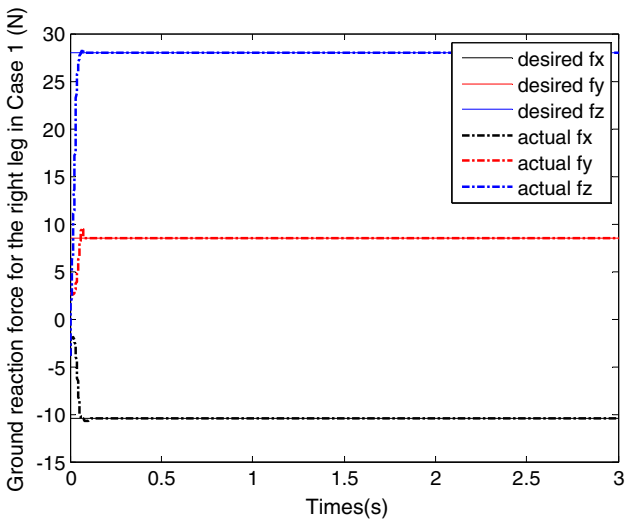

Fig. 5 Ground reaction force for the right leg in Case 1

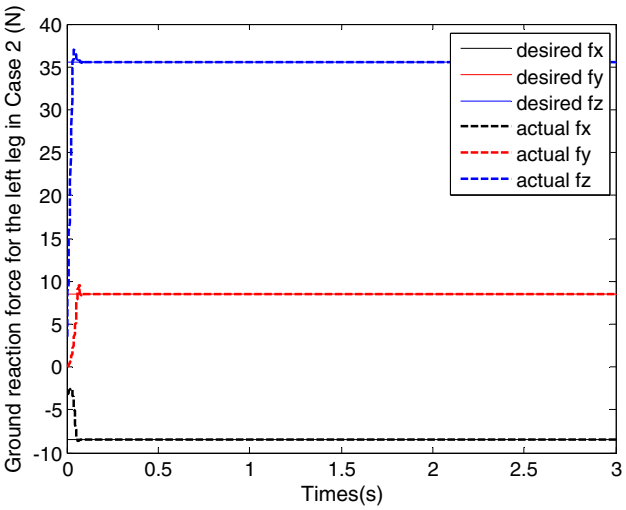

Fig. 6 Ground reaction force for the left leg in Case 2

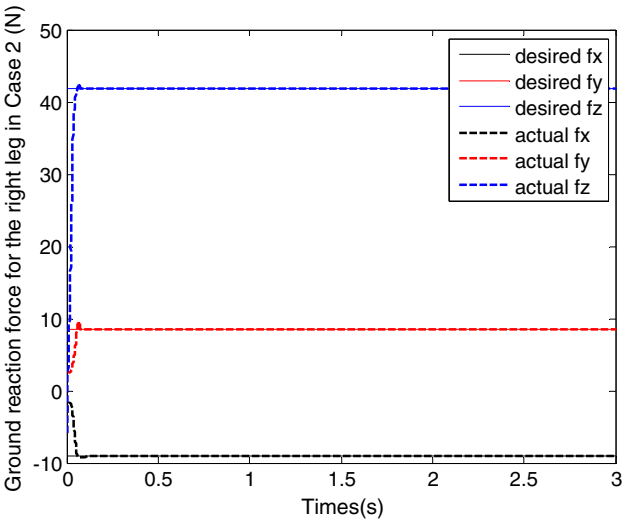

Fig. 7 Ground reaction force for the right leg in Case 2

are shown in Figs. 12 and 13. The simulation results indicate that the simulated biped robot remains dynamical balance under diverse perturbing external forces, which validate the effectiveness of the control law in Theorem 4.1. The proposed control scheme achieves good performance, which is mainly due to the "adaptive" mechanism, even if the nominal dynamics are uncertain. Although the parametric uncertainties and the external disturbances are both introduced into the simulation model, the force/motion control performance of system, under the proposed control, is not degraded. The simulation results demonstrate the effectiveness of the proposed adaptive control in the presence of unknown nonlinear dynamics and environments.

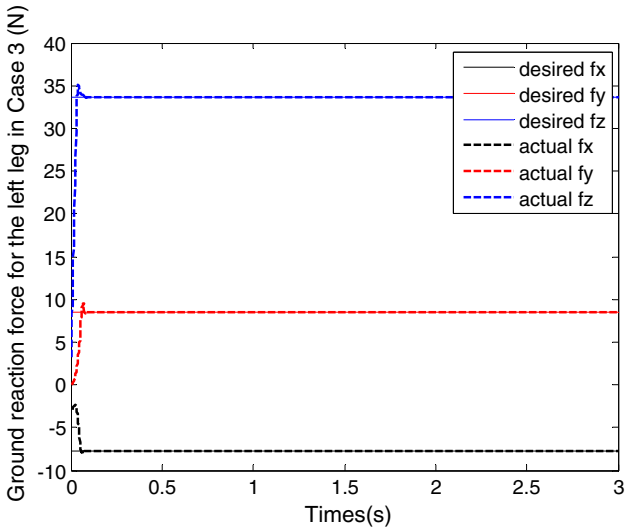

Fig. 8 Ground reaction force for the left leg in Case 3

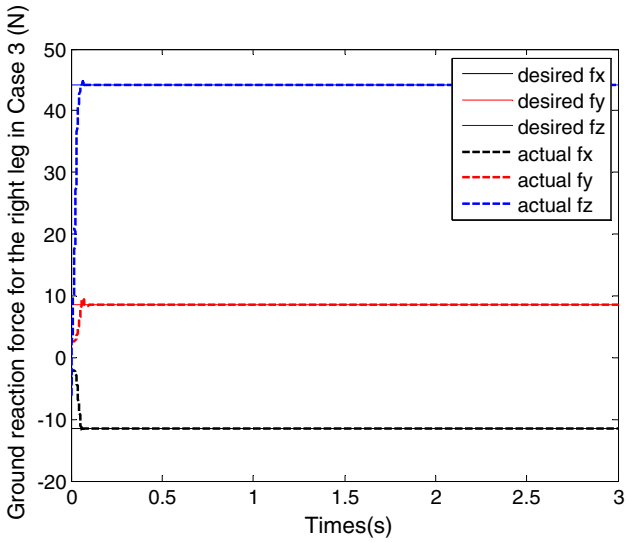

Fig. 9 Ground reaction force for the right leg in Case 3

5.2 Experiments

Experiments are carried out on a physical robot "Alpha". Alpha is a mini-type humanoid robot that is built at the Department of Electronic Engineering, Shunde Polytechnic, Guangdong of China. Alpha has 18 degree of freedom with a 0.394 m height and a 1.7 kg weight. The mechanical structure of the robot is shown in Fig. 14.

The biped carries a control board for controlling and communicating, a lithium-polymer battery in the robot's upper body for the servo motors. A RS-232 wireless transmission link connects the control software, which is running on a PC, to the robot's control board. Degrees of freedom (DOFs) of Alpha are schematically shown in

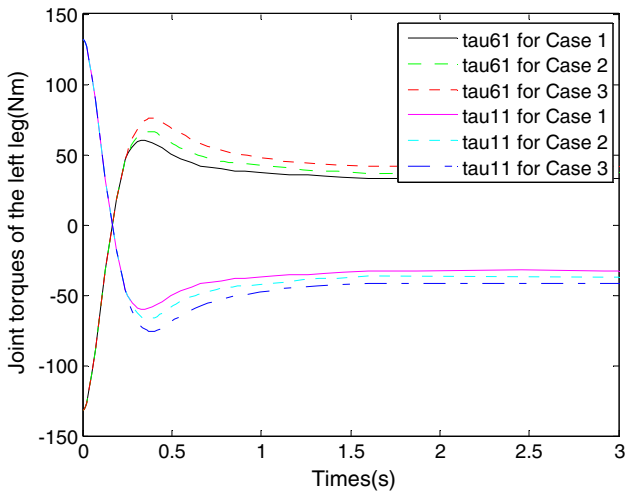

Fig. 10 Joint torques of the left leg in the three Cases

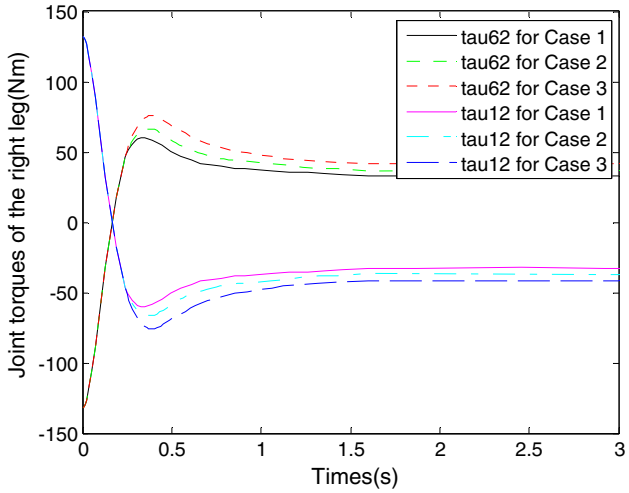

Fig. 11 Joint torques of the right leg in the three Cases

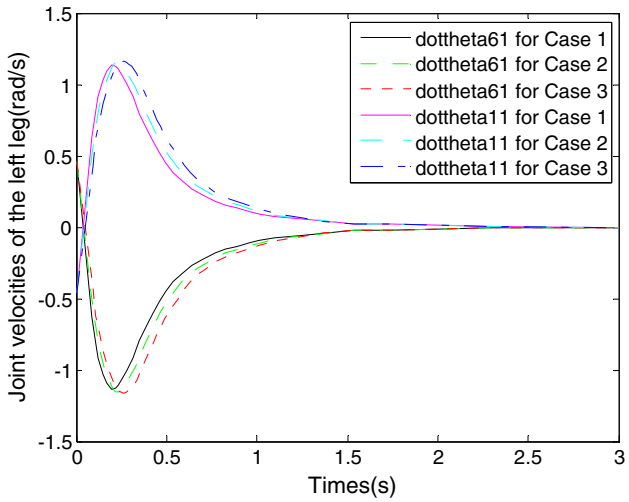

Fig. 12 Joint velocities of the left leg in the three Cases

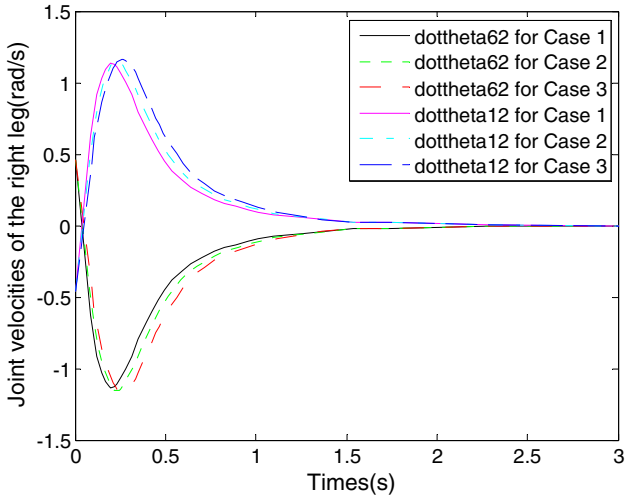

Fig. 13 Joint velocities of the right leg in the three Cases

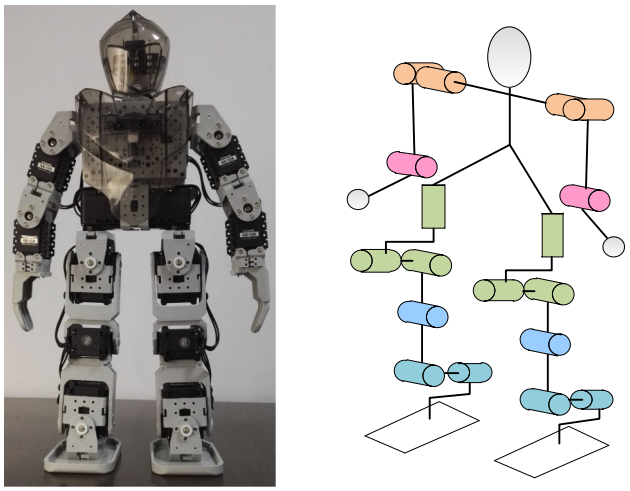

Fig. 14 The implemented prototype robot

Fig. 14. The robot is driven by 18 servo motors: six per leg and three in each arm. The six leg-servos allow for flexible leg movements: Three orthogonal servos constitute the 3-DOFs hip joint. Two orthogonal servos form the 2-DOFs ankle joint. One servo drives the knee joint. The sensors such as infrared sensors, force sensors and gyro sensors are interpreted to improve the ability of autonomous walking. Closed-loop control for the humanoid robot is constructed. Daily movements of Alpha, such as going straight, walking sideways, obstacle avoidance, and turning around, have been realized. The basic parameters of Alpha are shown in Table 1.

Continuous-force external disturbances are applied on the right shoulder of the biped robot until the joint angles of the hips and the ankles changed obviously. The disturbances are carried out by a hand of an experimenter. The

Table 1 Basic parameters of Alpha

Parameters	Value
Height (cm)	39.4
Weight (kg)	1.7
Degree of freedom	18

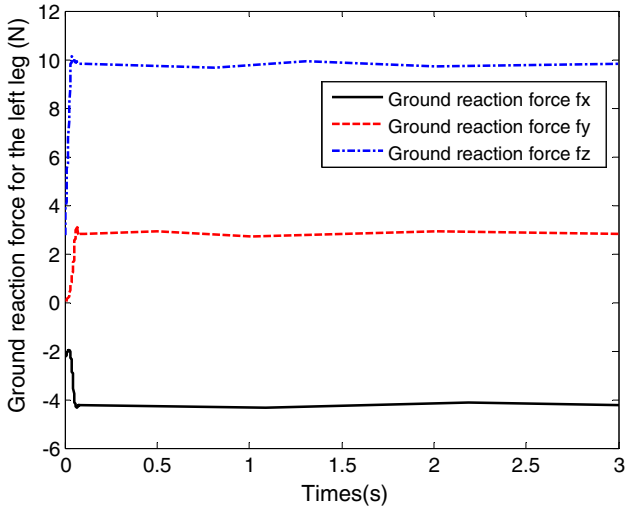

Fig. 15 Ground reaction force for the left leg of Alpha

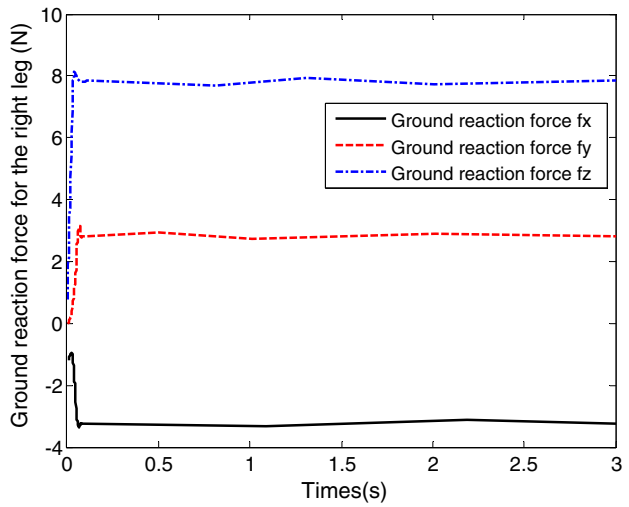

Fig. 16 Ground reaction force for the right leg of Alpha

ground reaction forces are measured via the pressure sensors embedded in each of the soles of the biped robot. As we can see from Figs. 15 and 16, ground reaction forces for the both legs become steady gradually under the proposed adaptive control. Figure 17 shows the snapshots of the biped under the implemented continuous-force external disturbances in double-support phase. After swaying smoothly to the left and then to the right, the prototype

Fig. 17 Snapshots for a biped robot in double-support phase under perturbing external forces

humanoid robot always restores the initial balance posture. The robot is able to react appropriately to the disturbances as desired. The experimental results show that the proposed adaptive control is effective.

6 Conclusions

In this paper, the dynamic balance optimization and control of biped robots have been investigated under the external disturbances in the double-support phase. First, a constrained dynamic model of the biped robot is formulated and a reduced order model for the double-support phase is derived. Then, a recurrent neural network has been adopted to deal with the complicated optimization problem subject to both equality and inequality constraints. For the given contact force and motion, we propose the hybrid motion/-force control based on Recurrent Neural Networks to approximate unknown dynamic functions, and the adaptive learning algorithms that can learn the parameters of the Recurrent Neural Networks are derived using Lyapunov stability theorem. The verification of the proposed control is conducted by simulations and experiments. We believe that the proposed method will be promising for dynamical balance optimization and control of biped robots under perturbing external forces.

Acknowledgments The authors would like to appreciate the editors and the reviewers for the constructive comments and suggestions. This work is supported by the National Natural Science Foundation of China under Projects 61403264 and 61305098.

References

1. Motoi N, Suzuki T, Ohnishi K (2009) A bipedal locomotion planning based on virtual linear inverted pendulum mode. IEEE Trans. Industrial Eletronics 56(1):54–61
2. Braun DJ, Goldfarb M (2009) A control approach for actuated dynamic walking in biped robots. IEEE Trans. Robotics 25(6):1292–1303
3. Furusho J, Sano A (1990) Sensor-based control of a nine-link biped. Int J Robot Res 9(2):83–98
4. Vukobratovic M, Borovac B (2004) Zero-moment point thirty five years of its life. Int. J. Humanoid Robot 1(1):157–173
5. Harada K, Kajita S, Kaneko K, Hirukawa H (2003) ZMP analysis for arm/leg coordination. In: Proceedings of IEEE/RSJ international conference intelligent robots system, Las Vegas, NV, pp 75–81
6. Hirai K, Hirose M, Haikawa Y, Takenaka T (1998) The development of Honda humanoid robot. In: Proceedings of IEEE international conference on robotics automation, Leuven, Belgium, vol 2, pp. 1321–1326
7. Setiawan S, Hyon S, Yamaguchi J, Takanishi A (1999) Physical interaction between human and a bipedal humanoid robot-realization of human-follow walking. In: IEEE international conference on robotics and automation, pp 361–367
8. Liu Z, Xu S, Zhang Y, Chen X, Chen CLP (2014) Interval type-2 fuzzy kernel based support vector machine algorithm for scene classification of humanoid robot. Soft Comput 18(3):589–606
9. Kuffner JJ, Kagami S, Nishiwaki K, Inaba M, Inoue H (2002) Dynamically-stable motion planning for humanoid robots. Auton Robots 12:105–118
10. Manchester IR, Mettin U, Iida F, Tedrake R (2011) Stable dynamic walking over uneven terrain. Int J Robot Res 30(3):265–279
11. Lim S, Oh SN, Kim KI (2012) Balance control for biped walking robots using only zero-moment-point position signal. Eletron Lett 48(1):19–20
12. Ge SS, Li Z (2012) Data driven adaptive predictive control for holonomic constrained under-actuated biped robots. IEEE Trans Control Syst Technol 20(3):787–795
13. Cui R, Yan W (2012) Mutual synchronization of multiple robot manipulators with unknown dynamics. J Intell Rob Syst 68(2):105–119
14. Cui R, Ren B, Ge SS (2012) Synchronised tracking control of multi-agent system with high-order dynamics. IET Control Theory Appl 6(5):603–614
15. Cui R, Yan W, Xu D (2012) Synchronization of multiple autonomous underwater vehicles without velocity measurements. Sci China Inf Sci 55(7):1693–1703
16. He W, Zhang S, Ge SS (2014) adaptive control of a thruster assisted position mooring system. Automatica 50(7):1843–1851
17. Zhao Z, He W, Ge SS (2014) Adaptive neural network control of a fully actuated marine surface vessel with multiple output constraints. IEEE Trans Control Syst Technol 22(4):1536–1543
18. He W, Zhang S, Ge SS (2014) Adaptive boundary control of a nonlinear flexible string system. IEEE Trans Control Syst Technol 22(3):1088–1093

19. Li Z, Yang C (2012) Neural-adaptive output control of a class of transportation vehicles based on wheeled inverted pendulum models. IEEE Trans Control Syst Technol 20(6):1583–1591
20. Panteley E, Stotsky A (1993) Adaptive trajectory/force control scheme for constrained robot manipulators. Int J Adapt Control Signal Process 7(6):489–496
21. Wang L, Liu Z, Chen CLP, Zhang Y (2014) Interval type-2 fuzzy weighted support vector machine learning for energy efficient biped walking. Appl Intell 40(3):453–463
22. Li Z, Su C-Y (2013) Neural-adaptive control of single-master multiple slaves teleoperation for coordinated multiple mobile manipulators with time-varying communication delays and input uncertainty. IEEE Trans Neural Netw Learn Syst 24(9): 1400–1413
23. Li Z, Kang Y (2010) Dynamic coupling switching control incorporating support vector machines for wheeled mobile manipulators with hybrid joints. Automatica 46(5):785–958
24. Aoi S, Tsuchiya K (2005) Locomotion control of a biped robot using nonlinear oscillators. Auton Robots 19:219–232
25. Freidovich LB, Mettin U, Shiriaev AS, Spong MW (2009) A Passive 2-DOF walker: hunting for gaits using virtual holonomic constraints. IEEE Trans. Robot 25(5):1202–1208
26. Grizzle JW, Abba G, Plestan F (2001) Asymptotically stable walking for biped robots: analysis via systems with impulse effects. IEEE Trans Autom Control 46(1):51–64
27. Plestan F, Grizzle JW, Westervelt ER, Abba G (2003) Stable walking of a 7-DOF biped robot. IEEE Trans Robot Autom 19(4):653–668
28. Ferreira JP, Crisostomo MM, Coimbra AP, Ribeiro B (2009) Control of a biped robot with support vector regression in sagittal plane. IEEE Trans Instrum Measure 58(9):3167–3176
29. Morimoto J, Atkeson CG (2007) Learning biped locomotion. IEEE Robot Autom Mag 14(2):41–51
30. Juang J (2000) Fuzzy neural network approaches for robotic gait synthesis. IEEE Trans Syst Man Cybern B Cybern 30(4):594–601
31. Wang L, Liu Z, Chen CLP, Zhang Y, Lee S, Chen X (2013) Fuzzy SVM learning control system considering time properties of biped walking samples. Eng Appl AI 26(2):757–765
32. Wang L, Liu Z, Chen PCL, Zhang Y, Lee S, Chen X (2013) A UKF-based predictable SVR learning controller for biped walking. IEEE Trans Syst Man Cybern Syst 43(6):1440–1450
33. Li Z, Ge SS, Liu S (2014) Contact-force distribution optimization and control for quadruped robots using both gradient and adaptive neural networks. IEEE Trans Neural Netw Learn Syst 25(8): 1460–1473
34. Li Z, Xia Y, Su C-Y, Deng J, Fu J, He W (2015) Missile guidance law based on robust model predictive control using neural network optimization. IEEE Trans Neural Netw Learn Syst. doi:10.1109/TNNLS.2014.2345734
35. Shih C, Gruver WA (1992) Control of a biped robot in the double-support phase. IEEE Trans Syst Man Cybern 22(4): 729–735
36. Luenberger DG (1984) Linear and nonlinear programming, 2nd edn. Addison-Wesley, Reading
37. Ge SS, Lee TH, Harris CJ (1998) Adaptive neural network control of robot manipulators. World Scientific, London
38. Lin F, Shieh H, Shieh P, Shen P (2006) An adaptive recurrent-neural-network motion controller for X-Y table in CNC machine. IEEE Trans Syst Man Cybern B 36(2):286–299
39. Li Z, Xia Y (2014) Adaptive neural network control of bilateral teleoperation with unsymmetrical stochastic delays and unmodelled dynamics. Int J Robust Nonlinear Control 24(11): 1628–1652
40. Li Z, Yang K, Bogdan S, Xu B (2013) On motion optimization for robotic manipulators with strong nonlinear dynamic coupling using support area level set algorithm. Int J Control Autom Syst 11(6):1266–1275
41. Li Z, Chen W (2008) Adaptive neural-fuzzy control of uncertain constrained multiple coordinated nonholonomic mobile manipulators. Eng Appl Artif Intell 21(7):985–1000
42. Li Z, Yang C (2007) Neuro-adaptive compliant force/motion control for uncertain constrained wheeled mobile manipulator. Int J Robot Autom 22(3):206–214